I-5-05 (Late News)

Light- and Heavy-Hole Valence Bands of Si/Si$_{0.7}$Ge$_{0.3}$ Nanopillars Fabricated by Neutral Beam Etching

Min-Hui Chuang[1,2], Yiming Li[1-3,*], and Seiji Samukawa[3,4]

[1] Parallel and Scientific Computing Laboratory; [2] Institute of Communications Engineering;
[3] Department of Electrical and Computer Engineering, National Chiao Tung University
1001 Ta-Hsueh Rd., Hsinchu City, Hsinchu 300, Taiwan
[4] Institute of Fluid Science, Tohoku University, 2-1-1 Katahira, Aoba-ku, Sendai, 980-8577, Japan
* Phone: +886-3-5712121 ext. 52974; Fax: +886-3-5726639; Email: ymli@faculty.nctu.edu.tw

Abstract

In this work, we discuss the geometry effect on the electronic structure for holes of the well-aligned silicon (Si) nanopillars (NPs) embedded in Si$_{0.7}$Ge$_{0.3}$ matrix fabricated by neutral beam etching. We formulate and solve the Schrödinger equation with an effective mass approach using 3D finite-element method in k space, which enables us to study the light- and heavy-hole valence bands. The effects of the height, radius, and separation of Si NPs on the energy band and density of states are investigated. The radius and separation of Si NPs play crucial roles in tuning hole valence bands.

1. Introduction

Silicon (Si) nanostructures have been of great interest for more than Moore applications, such as quantum dots (QDs) for intermediate band solar cells (IBSCs) [1-2] and nanopillars (NPs) for thermoelectric devices [3-4]. The neutral beam etching combined with bio-template technique [4] is a way to fabricate Si NPs with high density, period, and uniformity. In contract to real-space simulation of Si QDs for IBSCs [5], we explore Si/Si$_{0.7}$Ge$_{0.3}$ NPs by solving 3-D Schrödinger equation in k space for the thermoelectric applications. This study is useful to explore the number of conducting channels and the electrical conductivity [3].

2. Sample Fabrication and Simulation

The fabrication process of Si NPs embedded in Si$_{0.7}$Ge$_{0.3}$ has been proposed [4]; it starts from forming the thin oxide layer, which is also regarded as a part of mask in this fabrication process. The solution containing PEG-ferritin is dropped onto the sample and is used to form a uniform coating by spin coating at 2900 rpm. The protein shell is removed under the 673-K annealing. After the annealing, the surface oxide layer is etched using NF$_3$/H radicals. The chlorine NB is used to form Si NPs with a depth of 90 nm. After etching process, the mask will be removed and Si$_{0.7}$Ge$_{0.3}$ is epitaxially grown on the Si NP surface by thermal CVD. The schematic plot of the fabrication process is in Fig. 1(a). The SEM image for fabricated Si NPs is shown in Fig. 1(b). The fabricated Si NPs show a cylinder-like profile.

The energy band simulation is performed by solving the light- and heavy-hole Schrödinger equations in k space

$$\nabla[-\frac{\hbar^2}{2m^*}\nabla u_{n,k}(r)]-\frac{i\hbar^2}{m^*}k\cdot\nabla u_{n,k}(r)+[V(r)+\frac{\hbar^2 k^2}{2m^*}]u_{n,k}(r)=E_{n,k}\,u_{n,k}(r),\quad(1)$$

where $\hbar$ is the reduced Planck constant, m^* is 0.16m_0 (0.49m_0) and 0.10m_0 (0.41m_0) for light (heavy) holes in Si and Si$_{0.7}$Ge$_{0.3}$, respectively, V is the potential energy, $E_{n,k}$ is the quantum level, and $u_{n,k}(r)$ is the electron envelope function.
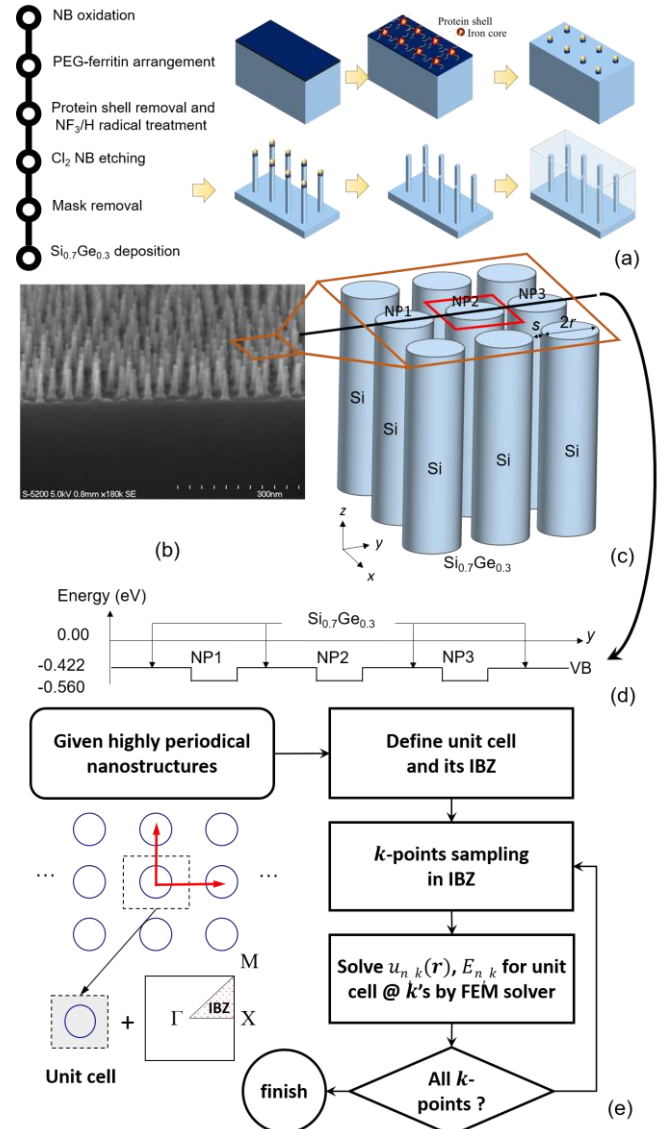

Fig. 1. (a) A schematic plot of the fabrication process. (b) The side view of the fabricated Si NPs [6]. (c) Illustration of the simulated structure, where r is the radius of Si NPs and s is the edge-to-edge separation. (d) The valence band (VB) edge of Si NPs embedded in Si$_{0.7}$Ge$_{0.3}$ matrix along y-axis cut from (c). Note that holes are confined in the VB of Si$_{0.7}$Ge$_{0.3}$. (e) The simulation flow for the electronic structure calculation for a given highly periodical nanostructure by introducing the concept of irreducible Brillouin zone (IBZ) in k space. For each sampling point in IBZ, the eigenvalue problem of Eq. (1) is solved by the finite-element (FEM) solver.
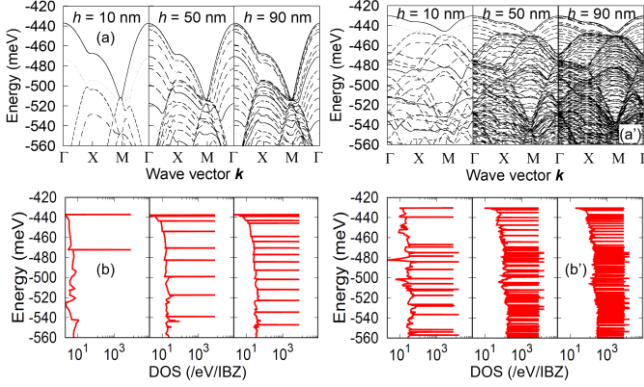
Fig. 2. The (a) energy band and (b) DOS of Si NPs for light hole with different h, where $r = 2$ nm and $s = 5$ nm are fixed. The (a') energy band and (b') DOS of the Si NPs for heavy hole under the same size. As h is increased, the number of bound states is increased due to the larger accommodation space.

Fig. 1(c) is a schematic plot of NPs; we model the structure as a superlattice with periodical boundary conditions on the sidewalls. The valence-band edges, cut from Fig. 1(c), is shown in Fig. 1(d). Fig. 1(e) describes the band structure calculation flow. We calculate the energy band at the sampling k point in the irreducible Brillouin zone (IBZ).

3. Results and Discussion

We consider heights (h), radii (r), and separations (s) to discuss the geometry effect on the light- and heavy-hole valence bands of Si NPs embedded in $Si_{0.7}Ge_{0.3}$ matrix. First, the energy band and the density of states (DOS) of Si NPs for different h, where $r = 2$ nm and $s = 5$ nm are fixed, are plotted in Fig. 2. The ground-state energy for heavy holes is higher than that of light holes, as shown in Figs. 2(a) and (a'). Furthermore, the number of bound states for heavy holes is larger than that of light holes due to the larger effective mass. As h is increased, the numbers of bound states for both light and heavy holes are increased due to the larger accommodation space, as shown in Figs. 2(b) and (b'). However, in the valence band, the highest quantized state has almost no change among all heights. Notably, not shown here, if Si NPs are embedded entirely in $Si_{0.7}Ge_{0.3}$ matrix, the effect of height on the quantized valence bands can be enhanced; such as the ground-state energy for light hole is with a 6-meV increase as h varies from 10 to 90 nm while that of heavy hole is with a 2-meV increase.

Second, the energy band and DOS of Si NPs for different r, where $s = 1$ nm and $h = 90$ nm are fixed, are plotted in Fig. 3. As r is increased, the Si barrier for holes becomes wider which makes the wave function inside $Si_{0.7}Ge_{0.3}$ matrix more difficult to penetrate into the Si barrier. Consequently, it will lead to a decreased ground-state energy when r is increased, as shown in Figs. 3(a) and (a'). Compared to Fig. 3(b), Fig. 3(b') shows that the variation of the highest ground-state energy is 15.7 meV for heavy holes when r varies from 0.5 to 1 nm which is smaller than that of light holes (19.3 meV) despite a larger accommodation states. The tunable range of light-hole subbands is more significant than that of heavy holes. Finally, the energy band and DOS of Si NPs with respect to different s, where $r = 2$ nm and $h = 90$ nm are fixed, are plotted in Fig. 4. As s is increased, the confinement potential for holes becomes wider; thus, the wave function is well confined in the $Si_{0.7}Ge_{0.3}$ matrix and a higher ground-
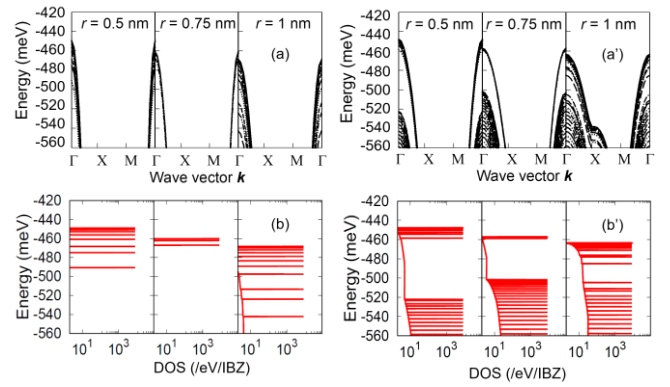

Fig. 3. The (a) energy band and (b) DOS of Si NPs for light hole with different r, where $s = 1$ nm and $h = 90$ nm are fixed. The (a') energy band and (b') DOS of the Si NPs for heavy hole under the same geometry condition. As r of Si NPs is increased, the barrier for holes is wider which makes the wave function more localized and lead to a decreased ground-state energy.
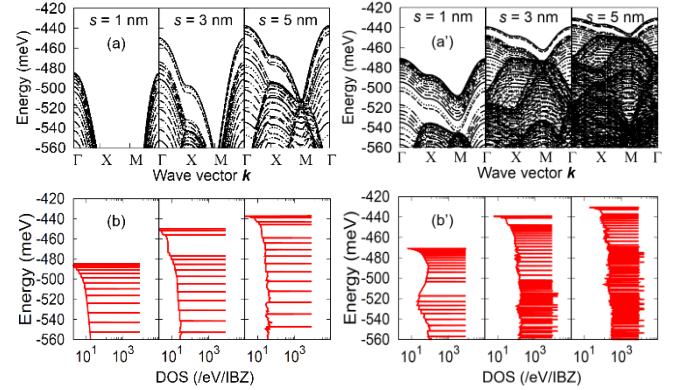

Fig. 4. The (a) energy band and (b) DOS of Si NPs for light hole with different s, where $r = 2$ nm and $h = 90$ nm are fixed. The (a') energy band and (b') DOS of Si NPs for heavy hole in the same geometry condition. As s is increased, the confinement potential for holes becomes wider; thus, the wave function is well confined in $Si_{0.7}Ge_{0.3}$ matrix and a larger ground-state energy is obtained.

state energy is obtained, as shown in Figs. 4(a) and (a'). Compared with Fig. 4(b), Fig. 4(b') shows that DOS for heavy holes is extremely increased as s is increased.

4. Conclusions

The electronic structure of Si nanopillars embedded in $Si_{0.7}Ge_{0.3}$ for holes with respect to different heights, radii, and separations has been discussed. The effect of the radius and separation on the hole energy band control are significant. We are currently applying these results to calculate the number of conducting channels and the electrical conductivity.

References

[1] M.-Y. Lee et al., IEEE Trans. Electron Devices **62** (2015) 3709.
[2] Y.-C. Tsai et al., Jpn. J. Appl. Phys. **55** (2016) 04EJ14.
[3] M.-Y. Lee et al., IEEE Trans. Electron Devices **67** (2020) 2088.
[4] A. Kikuchi et al., J. Appl. Phys. **122** (2017) 165302.
[5] W. Hu et al., IEDM, Dec. 10-12, 2012, pp. 6.1.1-6.1.4.
[6] M.-H. Chuang et al., Vacuum **181** (2020) 109577.